



## Glass formation and the structural study of the $\text{Sb}_2\text{O}_3\text{-SbPO}_4\text{-WO}_3$ system

Douglas Faza Franco<sup>1</sup>, Hssen Fares<sup>1</sup>, Antônio Eduardo de Souza<sup>1</sup>, Silvia Helena Santagneli<sup>2</sup>, Marcelo Nalin<sup>1+</sup>

<sup>1</sup> São Paulo State University (Unesp), Institute of Chemistry, Department of General and Inorganic Chemistry, 55 Prof. Francisco Degni St, Araraquara, São Paulo 14800-060, Brazil

<sup>2</sup> São Paulo State University (Unesp), Institute of Chemistry, Department of Physical Chemistry, 55 Prof. Francisco Degni St, Araraquara, São Paulo 14800-060, Brazil

+ Corresponding author: Marcelo Nalin, phone: +55-16-3301-9560, e-mail address: [mnalin@iq.unesp.br](mailto:mnalin@iq.unesp.br)

### ARTICLE INFO

Article history:

Received: October 09, 2017

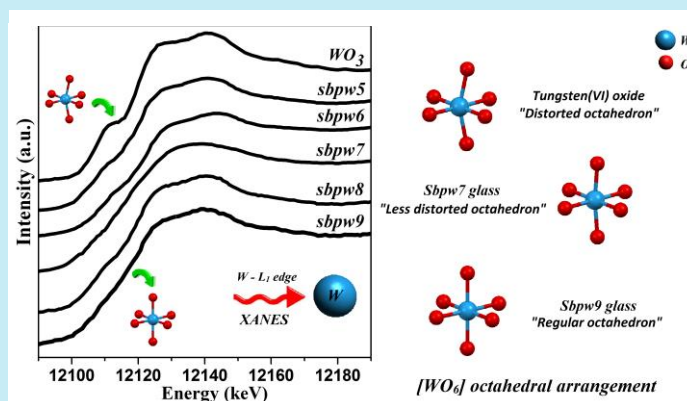
Accepted: November 27, 2017

Published: December 30, 2017

Keywords:

1. Antimony
2. Tungsten
3. Glasses
4. Raman spectroscopy
5. Structural properties

**ABSTRACT:** Glasses in the ternary system  $(\text{Sb}_2\text{O}_3)_{(0.6-x)}(\text{SbPO}_4)_{(0.4)}(\text{WO}_3)_x$ , with composition  $0.1 \leq x \leq 0.5$  (in mol %) were studied. The structural changes due to the replacement of  $\text{Sb}_2\text{O}_3$  by  $\text{WO}_3$  have been investigated. It was found that the incorporation of  $\text{WO}_3$  enhances the thermal stability of the glasses against devitrification when compared to the binary  $\text{Sb}_2\text{O}_3(0.6) - \text{SbPO}_4(0.4)$  composition. The connectivity of the network increases with  $\text{WO}_3$  content which is consistent with the high values of the glass transition temperature. Raman studies suggest that  $\text{WO}_3$  incorporation breaks the primary network, constituted by antimony oxide, while a second network containing  $\text{WO}_6$  octahedral units is built up. Thermal and structural properties were evaluated by differential scanning calorimetry, infrared and Raman spectroscopies, <sup>31</sup>P Magic Angle Spinning NMR and X-ray absorption near edge structure (XANES) at  $L_1$  and  $L_3$  edges of Sb and  $L_1$  edge of W atoms.



### 1. Introduction

Antimony oxide based glasses have been the subject of interesting studies in the last years<sup>1-11</sup> and have been claimed to be useful in important fields of the materials science, such as photonics<sup>12-16</sup> and plasmonics<sup>17-19</sup>. These materials present low phonon energy ( $\sim 600\text{-}700\text{ cm}^{-1}$ ) due to low energy stretching vibrations of Sb-O-Sb band<sup>20,21</sup>, high linear and non-linear refractive indexes<sup>3-5</sup> and the possibility of modulation of their optical constants, (refractive index,  $n$ , and absorption coefficient,  $\alpha$ ) under laser irradiation<sup>22</sup> what make them promising materials for

3D optical storage<sup>23,24</sup> as well as, for holographic data storage<sup>25</sup>.

Recently, some papers have demonstrated that the addition of  $\text{WO}_3$  can improve considerably the thermal stability against devitrification, non-linear and photosensitive properties of oxide and fluorophosphate glasses<sup>26-28</sup>. In order to improve the photosensitive and optical properties of Sb-based glasses,  $\text{WO}_3$  was added to the binary system  $\text{Sb}_2\text{O}_3\text{-SbPO}_4$ . Such system was previously characterized with respect to its thermal, and structural properties<sup>4</sup>, as well as, by their photosensitive response under laser irradiation<sup>29</sup>.

Considering both, antimony and tungsten glasses, the comprehension of the special properties of such materials requires a detailed description of the structure of the glass network. In this paper, a systematic structural investigation of the glass series  $(0.6-x)\text{Sb}_2\text{O}_3\text{-}0.4\text{SbPO}_4\text{-}x\text{WO}_3$  (with  $0.1 \leq x \leq 0.5$  in mol%) was performed using thermal analysis, FTIR, Raman,  $^{31}\text{P}$  magic angle spinning Nuclear Magnetic Resonance (MAS) NMR spectroscopies and X-ray absorption near edge structure (XANES) recorded at  $\text{Sb-L}_1$  and  $\text{Sb-L}_3$  edges as well as at the  $\text{W-L}_1$  edge.

## 2. Experimental

### 2.1. Glass preparation

Starting materials used for glass synthesis were  $\text{Sb}_2\text{O}_3$ ,  $\text{WO}_3$  (grade purity 99%) and  $\text{SbPO}_4$ , prepared as reported previously<sup>1</sup>. Syntheses were carried out by melting starting materials in glassy carbon crucibles in electrical furnace for 10 min between 800 and 1100 °C, depending on the glass composition, under a constant flow of  $\text{N}_2$ . The melts were cast and glass samples were obtained upon cooling. For less stable glasses, melts were quenched between two copper plates leading to samples around 1 mm in thickness. For more stable compositions, samples with 10 mm in thickness were obtained. For bulk synthesis, the melt was poured into a pre-heated mold (at  $T_g - 10$  °C) and kept 2 h at this temperature for annealing. This procedure was done in order to eliminate the residual stress induced by the quenching process.

### 2.2. Characterization

Characteristic temperatures of the glasses, glass transition ( $T_g$ ), onset of crystallization ( $T_x$ ), maximum of crystallization ( $T_p$ ) and thermal stability parameter ( $T_x - T_g$ ) were obtained by differential scanning calorimetry, using a Seiko SSC/5200 calorimeter with heating rate of 10 °C  $\text{min}^{-1}$ , under  $\text{N}_2$  atmosphere. The experimental errors for characteristic temperatures are 2 °C for  $T_g$  and  $T_x$  and 1 °C for  $T_p$ .

X-ray diffraction (XRD) was used to confirm the amorphous character and was performed using a Siemens Crystalloflex Diffractometer with  $\text{CuK}\alpha$  radiation equipped with a Ni filter, in the  $2\theta$  range from 4 to 70 degrees.

FTIR (Fourier Transform InfraRed) spectroscopy was performed using a Perkin Elmer FT-IR Spectrum 2000 from powdered glasses dispersed in KBr pellets,

operating at wavenumbers ranging from 400 to 4000  $\text{cm}^{-1}$ .

Raman scattering spectra, recorded from 200 to 1300  $\text{cm}^{-1}$  were obtained from the powdered glasses using a Micro-Raman Renishaw, equipped with a microscope, using He/Ne laser excitation (632.5 nm) with 30 mW CW power and a spot size around 5  $\mu\text{m}$ . The deconvolutions of the samples sbpw5 and sbpw9 were done using Gaussian functions.

Solid state  $^{31}\text{P}$  MAS-NMR spectroscopy was used to characterize the local phosphorous environment. The glasses were crushed and ground into powders before filling a zirconia tube.  $^{31}\text{P}$  solid state NMR spectra were obtained on an INOVA Varian-300 spectrometer, operated at a spinning frequency of 6 kHz at pulse length of  $\pi/2$  and a repetition time between each acquisition of 100 s. Chemical shifts were referenced to an external sample of 85%  $\text{H}_3\text{PO}_4$  solution.

XANES at the  $\text{Sb-L}_1$  and  $\text{L}_3$  edges, as such as, at  $\text{W-L}_1$  measurements have been carried out at LURE (Orsay, France) on the D44 bean line using a Si (111) double crystal monochromator detuned by 60 % in order to reject the harmonics. Measurements have been done in TEY (Total Electron Yield) mode. Energy calibration has been checked by using a Titanium foil (4966.0 eV) recorded between each glassy sample.  $\text{Sb-L}_3$  edge (4132 eV) spectra were collected over 340 eV with an energy step of 0.3 eV and counting time of 3 s whereas  $\text{Sb-L}_1$  edge spectra (4698 eV) were recorded over 100 eV with an energy step of 0.3 eV and counting time of 1 s.  $\text{W-L}_1$  edge (10180 eV) spectra were collected over 180 eV with an energy step of 0.5 eV and counting time of 3 s. For each sample several scans were recorded to improve the signal-to-noise ratio.  $\text{Sb}_2\text{O}_3$ ,  $\text{SbPO}_4$  and  $\text{WO}_3$  powdered samples prepared as pellets were recorded in TEY as reference compounds. XANES data analysis from  $\text{W-L}_1$ ,  $\text{Sb-L}_1$  and  $\text{L}_3$  edges were done subtracting the absorption background from the rough spectra using a linear function. Then, the spectra were normalized far from the edge in a range of pure atomic absorption.

## 3. Results and discussion

### 3.1. Thermal analysis

Stable compositions against devitrification have been obtained into the ternary  $\text{Sb}_2\text{O}_3\text{-SbPO}_4\text{-WO}_3$  glass system. Figure 1 illustrates the glass-forming domain for the system and the glass-forming region appears like a hatched green color area. All samples shown in

the diagram were obtained by fast quenching. Glasses containing less than 40 mol% in  $\text{WO}_3$  are yellow, while dark green colours are observed for higher concentrations. X-ray powder diffraction of the glasses confirms the amorphous character of the samples showing the characteristic broad diffraction profile halo (not shown here).

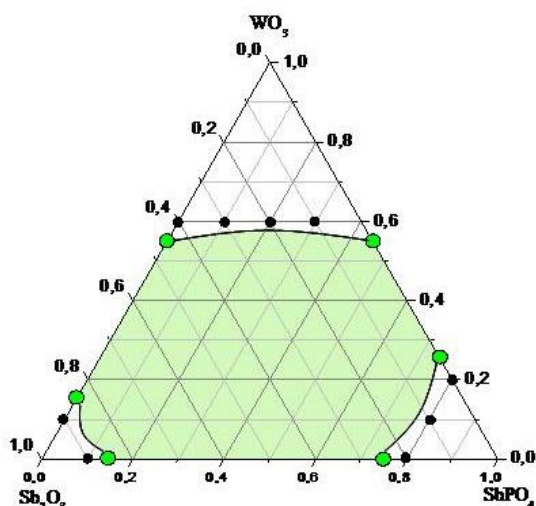


**Figure 1.** Glass domain of  $\text{Sb}_2\text{O}_3$ - $\text{SbPO}_4$ - $\text{WO}_3$  system. Hatched grey region refers to glassy compositions. Black dots represent ceramic compositions.

**Table 1.** Composition and characteristic temperatures of the glass samples for the three series studied

Samples	Composition (mol%)			Characteristic Temperatures ( $^{\circ}\text{C}$ )			
	$\text{Sb}_2\text{O}_3$	$\text{SbPO}_4$	$\text{WO}_3$	$T_g$	$T_x$	$T_p$	$T_x-T_g$
sbpw1	40	10	50	379	441	460	62
sbpw2	40	20	40	369	436	464	67
sbpw3	40	30	30	360	458	492	98
sbpw4	40	50	10	342	443	465	101
sbpw5	10	40	50	436	535	542	99
sbpw6	20	40	40	396	524	542	128
sbpw7	30	40	30	370	499	509	129
sbpw8	40	40	20	346	477	492	131
sbpw9	50	40	10	329	470	492	141
sbpw10	80	10	10	287	344	357	57
Sbpw11	70	20	10	300	373	392	73
sbpw12	60	30	10	319	411	441	92
sbpw13	30	60	10	346	435	449	89

Thermal analysis (Figure 2a) shows that the addition of  $\text{WO}_3$  increases  $T_g$  almost linearly for all compositions. On the other hand, while  $T_x-T_g$  increases for the sample containing 10 mol % of  $\text{WO}_3$ , further addition of tungsten oxide decreases the thermal stability. Classically,  $T_x-T_g$  have been used for comparison purposes in order to determine the most stable composition in a given glass system<sup>30</sup> and it states that higher is the difference lower is the tendency to devitrification. The relationship between  $T_g$  and the

Glass compositions, characteristic temperatures of the glasses, as well as, the stability parameter ( $T_x-T_g$ ) are summarized in the Table 1.  $T_x-T_g$  is the parameter commonly used to estimate the thermal stability of the glasses against devitrification. Usually, values higher than  $100\text{ }^{\circ}\text{C}$  enable the preparation of large samples. In this work, glasses containing 40 mol% of  $\text{SbPO}_4$  showed to be the most stable compositions with  $T_x-T_g$  value of  $141\text{ }^{\circ}\text{C}$  for the composition  $50\text{Sb}_2\text{O}_3$ - $40\text{SbPO}_4$ - $10\text{WO}_3$ . Due to the higher thermal stability of the compositions containing 40 mol% of  $\text{SbPO}_4$ , the series  $(\text{Sb}_2\text{O}_3)_{(0.6-x)}(\text{SbPO}_4)_{(0.4)}(\text{WO}_3)_x$  was chosen to study the influence of the substitution of  $\text{Sb}_2\text{O}_3$  by  $\text{WO}_3$ , with respect to the structural changes in the glassy network.

content of  $\text{WO}_3$  will be better discussed in the next section.

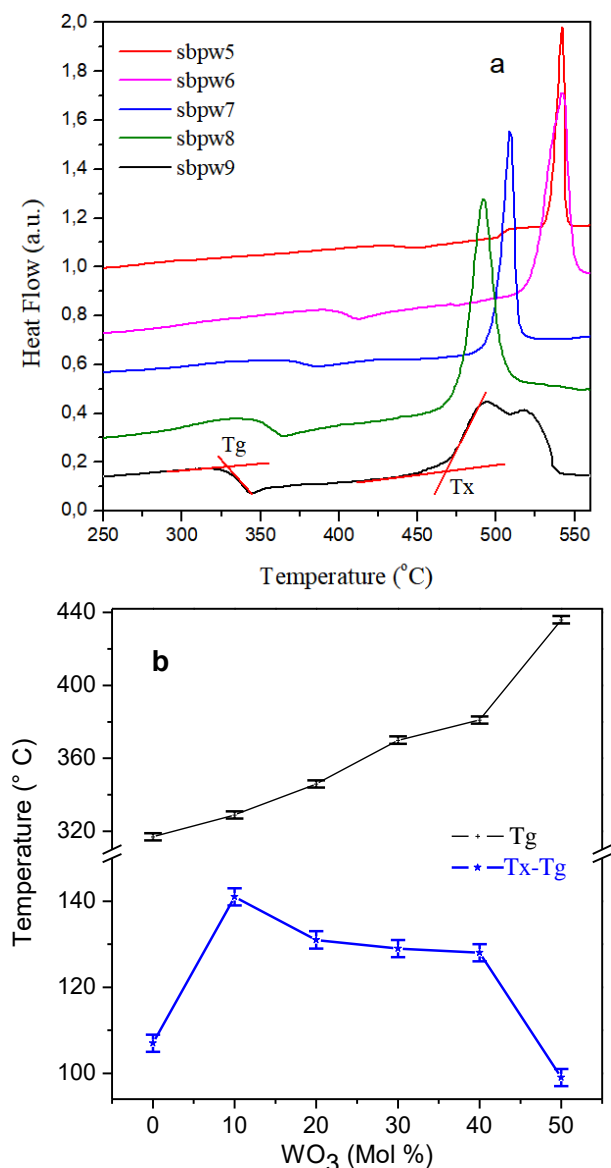


**Figure 2.** a) DSC curves for the compositions studied. b) Evolution of  $T_g$  and  $T_x - T_g$  for  $(\text{Sb}_2\text{O}_3)_{(0.6+x)}(\text{SbPO}_4)_{(0.4)}(\text{WO}_3)_x$  glass samples. The 0 mol% corresponds to the data obtained for the binary glass system  $60\text{Sb}_2\text{O}_3\text{-}40\text{SbPO}_4$ . The lines connecting points are just guides for the eyes.

### 3.2. Infrared and Raman spectroscopies

FTIR spectra of the glasses are shown in Figure 3. The attributions of the bands were done based on the spectra of crystalline reference compounds, i.e.,  $\text{Sb}_2\text{O}_3$  (cubic, *c*, and orthorhombic, *o*, forms),  $\text{SbPO}_4$  and  $\text{WO}_3$  also presented in Figure 3. The broad absorption bands of the glass samples make difficult a quantitative assignment. The spectrum of sbpw9 (sample containing 10 mol% of  $\text{WO}_3$ ) presents two main absorption bands: the first one centered at about  $1010\text{ cm}^{-1}$  and the second

around  $610\text{ cm}^{-1}$ . The higher energy band includes three asymmetric and one symmetric stretching vibrations of  $\text{PO}_4$  units ( $1140$ ,  $1068$ ,  $1035$  and  $990\text{ cm}^{-1}$  respectively) as well as one weak shoulder corresponding to the vibrations of  $\text{W-O}_t$  (terminal) bonds ( $920\text{ cm}^{-1}$ ). On the other hand, the lower energy bands envelop the stretching modes from the  $\text{WO}_6$  units ( $\nu_{\text{as}}$   $815\text{ cm}^{-1}$  and  $\nu_{\text{s}}$  at  $780\text{ cm}^{-1}$ ), the bending mode  $\delta_{\text{as}}$  P-O-Sb ( $643\text{ cm}^{-1}$ ) from  $\text{SbPO}_4$  and the asymmetric stretching  $\nu_{\text{as}}$  Sb-O ( $544\text{ cm}^{-1}$ ) arising from  $\text{Sb}_2\text{O}_3$ . For glass samples, with increase of  $\text{WO}_3$  content (from sbpw9 to sbpw5), both bands become broader.

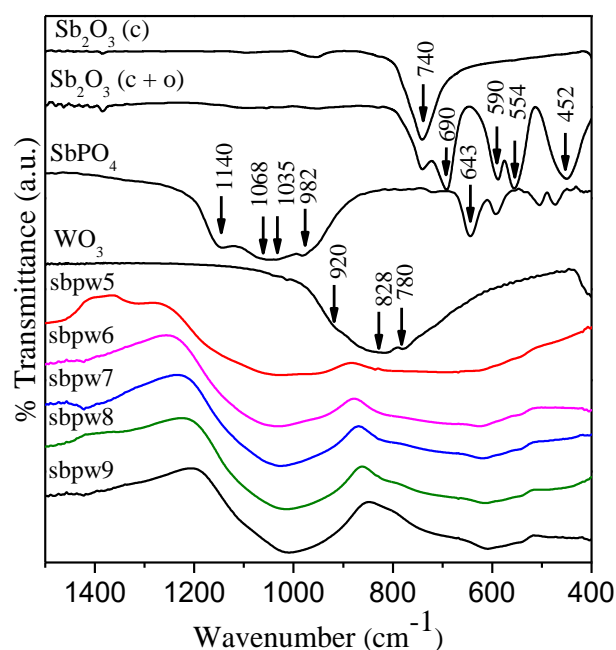


**Figure 3.** Infrared spectra of the reference compounds and glass samples. The curves were vertically translated for a better view.

In Figure 4a are shown the Raman spectra obtained for glasses and for reference compounds. Detailed assignments of the Raman bands for crystalline references were given elsewhere<sup>31</sup>. The intensities of the bands at  $205$  and  $440\text{ cm}^{-1}$  decrease with increasing  $\text{WO}_3$  content. A third band, appears at  $360\text{ cm}^{-1}$ , and its intensity increases for richer tungsten oxide samples. The two first bands were assigned to  $\text{SbO}_4$  and  $\text{SbO}_3$  units from  $\text{SbPO}_4$  and  $\text{Sb}_2\text{O}_3$  compounds respectively, while the band centered at  $360\text{ cm}^{-1}$  was assigned to bending of the W-O modes<sup>32</sup>. The band at  $815\text{ cm}^{-1}$  is characteristic of stretching W-O-W modes arising from  $\text{WO}_6$  octahedra and its intensity increases with  $\text{WO}_3$  content. A band, close to  $910\text{ cm}^{-1}$ , appears for all samples. This band has been attributed to  $(\text{W-O}_t)$

terminal bonds<sup>32</sup>. However, the  $\text{WO}_3$  monoclinic crystalline phase does not present such band, once, all corners of the  $\text{WO}_6$  polyhedron are shared with other five  $\text{WO}_6$  units.  $\text{W-O}_i^-$  band is present in compounds like  $\text{Na}_2\text{WO}_4$  and  $\text{Na}_2\text{W}_2\text{O}_7$ <sup>27,32</sup>. In  $\text{Na}_2\text{WO}_4$ , the W atoms are assumed to be in a tetrahedral environment of four oxygen atoms while in  $\text{Na}_2\text{W}_2\text{O}_7$  the tungsten atoms are in an octahedral geometry, however, in the last case, only the four oxygen atoms in the plane of the octahedral are bonded to other  $\text{WO}_6$  units, forming a linear-like chain. Indeed,  $\text{Na}_2\text{W}_2\text{O}_7$  presents vibrations like those observed for octahedral  $\text{WO}_6$

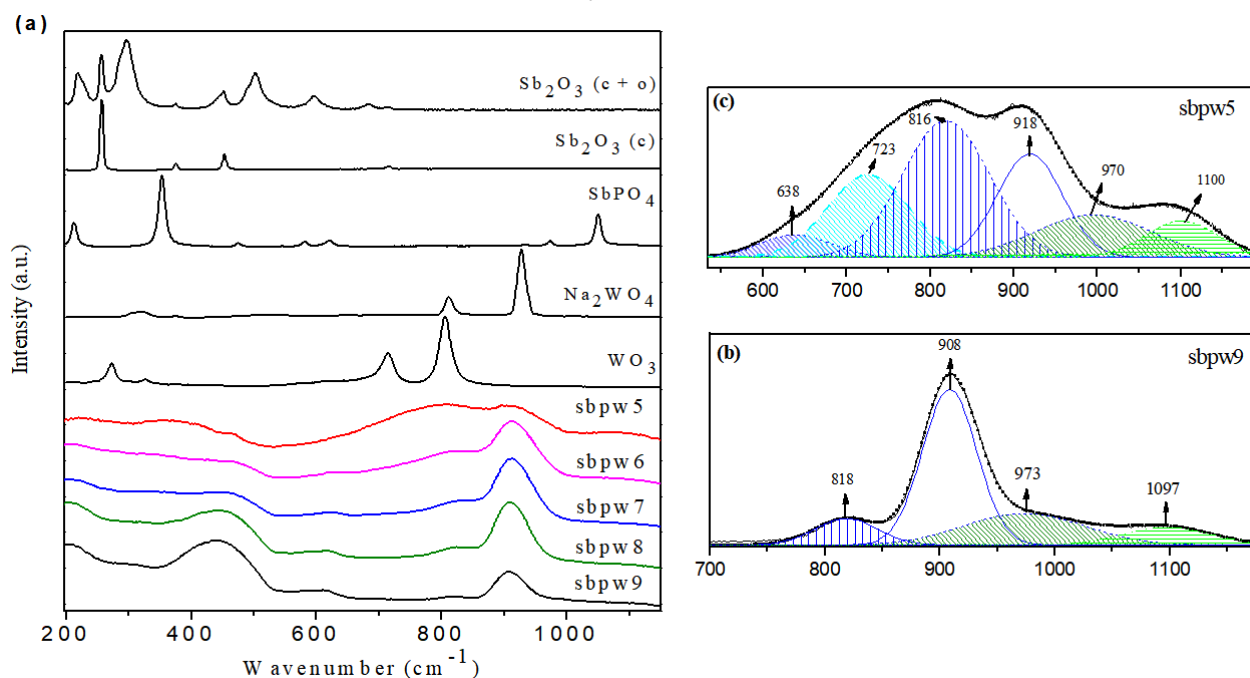


**Figure 4.** a) Raman spectra of glass samples and reference compounds. b) Gaussian deconvolution of the P-O and W-O Raman bands for sbpw9 (b) and sbpw5 (c) glasses. The curves were vertically translated for a better view.

### 3.3. $^{31}\text{P}$ MAS-NMR spectroscopy

$^{31}\text{P}$  MAS-NMR measurements of the crystalline antimony phosphate reference compound and glass compositions are shown in Figure 5. The  $\text{SbPO}_4$  crystalline is formed by  $\text{PO}_{4/4}$  units bonded by four  $\text{SbO}_{4/4}$  tetrahedra, forming P-O-Sb linkage and showing the chemical shift at -18.0 ppm. The spectra of the glasses present a broad lineshape near -13 ppm, characteristic of the  $\text{Q}_4$  phosphate units, which are linked to four antimony tetrahedra. The assignment was based on previous study in the  $\text{SbPO}_4\text{-WO}_3$  glass system<sup>30</sup> and the results show that the substitution of the  $\text{Sb}_2\text{O}_3$  by  $\text{WO}_3$  in the glassy matrix has no influence on the chemical environment of the  $\text{Q}_4$  phosphate units, which are bonded to four antimony tetrahedra

besides those present in tetrahedral  $\text{WO}_4$  units. It is needed to point out that both  $\text{W=O}$  and  $\text{W-O}^-$  are equivalent from the resonance point of view<sup>33</sup>. The intensity of the band at 910  $\text{cm}^{-1}$ , compared to that at 830  $\text{cm}^{-1}$ , decreases when the  $\text{WO}_3$  content rises up. In fact, the broad band observed for sbpw5 and extending from 550 to 1200  $\text{cm}^{-1}$  is the convolution of, at least, six distinct vibrations coming from tungsten oxide and antimony phosphate counterparts. Deconvolution of the lower (sbpw9) and upper (sbpw5) samples are shown in Figure 4b and 4c.

suggesting that  $\text{WO}_6$  units are randomly distributed in the network.

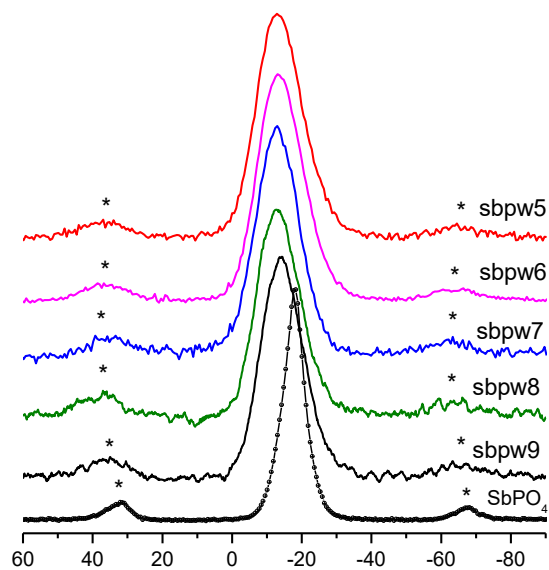


**Figure 5.**  $^{31}\text{P}$  NMR spectra of the glasses and the  $\text{SbPO}_4$  crystalline. The (\*) in the spectra are spinning sidebands. The curves were vertically translated for a better view.

### 3.4. X-ray absorption spectroscopies

Absorption data from Sb- $L_3$ -edge (Figure 6) refer to transition from  $2p_{3/2}$  level towards empty  $d$  and  $s$  states. The pre-peak in the rising edge ( $\sim 4138$  eV) is attributed to  $2p_{3/2} \rightarrow 5s\sigma^*$  transition, where  $\sigma^*$  designates the antibonding level related to the bonding level, which is responsible from the binding between Sb and O<sup>29</sup>. The vacant density of states at the  $5s\sigma^*$  level depends on the oxygen polyhedron around Sb (III). Indeed, the steric hindrance of the lone pair leads to a decrease in the vacant density of states for the  $5s\sigma^*$  level when the symmetry changes from  $\text{Sb}_2\text{O}_3$  (symmetry  $\text{SbO}_3\text{E}$ ) to  $\text{SbPO}_4$  (symmetry  $\text{SbO}_4\text{E}^-$ , where E represents the lone pair)<sup>4</sup>. Accordingly, the intensity of the pre-peak is lower for  $\text{SbPO}_4$  than for  $\text{Sb}_2\text{O}_3$ . The main absorption at higher energy (4145 eV) can be interpreted as a  $2p_{3/2} \rightarrow 5d$  transition. According to the Figure 6, no drastic change is observed in the pre-peak with increases of the  $\text{WO}_3$  content. These results support the observation done for  $^{31}\text{P}$  NMR and reinforce the hypothesis that the substitution of  $\text{Sb}_2\text{O}_3$  by  $\text{WO}_3$  does not influence the Sb environment significantly. The insert present in Figure 6 shows the typical absorption curves for Sb- $L_1$  edge. Absorption at Sb- $L_1$ -edge refers to transitions from  $2s$  level towards empty  $p$  states and are sensible to oxidation state of the cation. The peak centered at 4303 eV corresponds to  $\text{Sb}^{3+}$  species<sup>34</sup>. No absorption was found at 4707 eV indicating the absence of  $\text{Sb}^{5+}$  species in glasses.

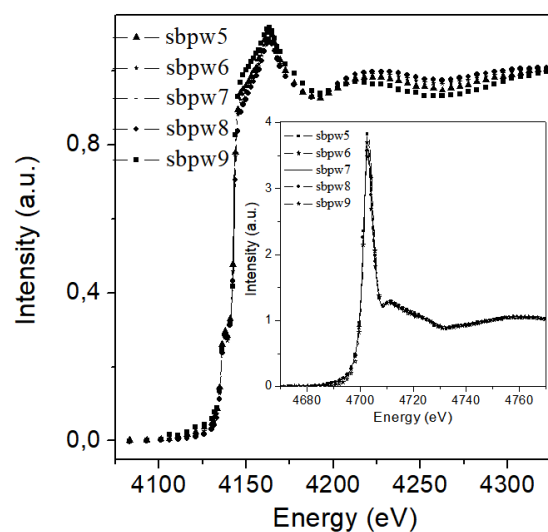


**Figure 6.** Sb  $L_3$ -edge spectra from glass samples. Insert: Sb  $L_1$ -edge spectra from glass samples showing only the presence of  $\text{Sb}^{3+}$  species.

XANES data at W- $L_1$  edge obtained for both glasses and reference compounds are shown in Figure 7. The main difference between  $\text{WO}_3$  and  $\text{Na}_2\text{WO}_4$  is the presence of the peak around 12108 eV which is attributed to the W ions in a tetrahedral environment in the sodium tungstate crystals<sup>32</sup> while, in tungsten oxide, W ions are surrounded by six oxygen atoms in a distorted octahedral structure. One must point out that, in both, tetrahedral and octahedral structures, W ions have the 6+ oxidation state. Results from Figure 7 suggest that the local structure around W for glasses is closest to that observed in  $\text{WO}_3$  crystals with distorted octahedral arrangement. In fact, by the analysis of the pre-peak of W- $L_1$  edge, it can be said that the  $\text{WO}_6$  units present in glasses are less distorted than those observed in  $\text{WO}_3$  crystals, supposing to be arranged in a less compact structure than that observed for crystalline  $\text{WO}_3$ .

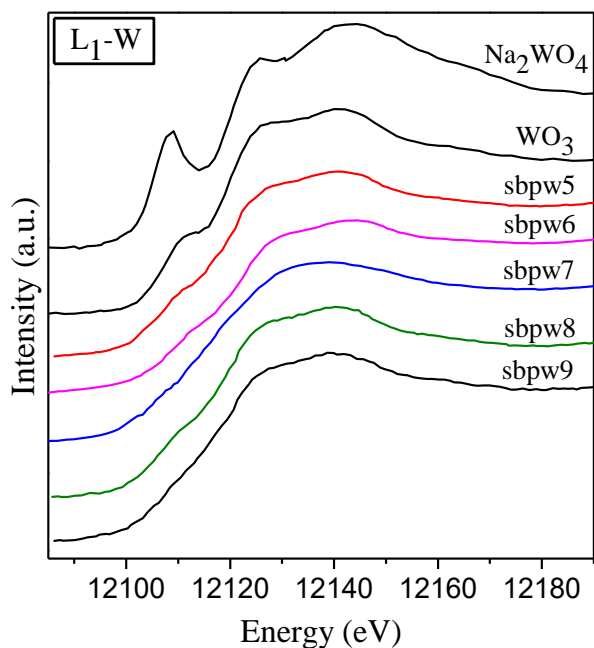


**Figure 7.** W- $L_1$  edge data from the glass samples and reference compounds. The weak shoulder absorption at 12108 eV is similar to that observed for crystalline  $WO_3$ .

#### 4. Discussion

The glasses in the series  $(Sb_2O_3)_{(0.6-x)}(SbPO_4)_{(0.4)}(WO_3)_x$  present good thermal properties. As observed in Figure 2b, the incorporation of  $WO_3$  into the binary  $Sb_2O_3$ - $SbPO_4$  system increases the glass transition temperature. In fact, with respect to  $T_g$ , it was verified that the subsequent addition of  $WO_3$  to the binary composition, raise up the values of  $T_g$  from 318 °C (binary) to 436 °C (sbpw5). This behavior may be a consequence of an increase of the connectivity and/or of the disorder of the glass network. Similar aspect was observed by M. Maczka et al., in cesium magnesium tungsten phosphate glasses<sup>35</sup>. The criterion to consider the structure more or less disordered comes from the fact that addition of  $WO_3$  to the binary system incorporates one more component in the glass composition what is consistent with the “confusion principle”, which states that the larger number of components in a glass system destabilizes competing crystalline phases which may forming during cooling<sup>36</sup>.

On the other hand, the behavior of  $T_x - T_g$  parameter is not regular. Compared to the binary, the  $T_x - T_g$  value for the sample containing 10 mol% of  $WO_3$ , jumps from 106 (binary) to 141 °C. However, for further  $WO_3$  contents,  $T_x - T_g$  decreases to 99 °C destabilizing the glass structure (sbpw5). It looks reasonable to assume that for sample sbpw16 the  $WO_6$

units are quite dispersed into the glass matrix. For samples with higher  $WO_3$  contents, the octahedral  $WO_6$  units begin to link to each other forming a parallel structure that is similar to that of the monoclinic form of  $WO_3$ . This affirmation is supported by infrared, Raman and W- $L_1$  XANES measurements and will be discussed below.

Although, the bands of the glasses in the infrared region present a broad profile, it is possible to notice that for sbpw16 sample the P-O stretching bonds, arising from orthophosphate, are slightly shifted to lower frequencies compared to the reference compound. This feature suggests that in the glassy form, the antimony orthophosphate is present in a less compact (or less connected) structure when the content of  $WO_3$  is low. However, increasing the  $WO_3$  content, the P-O bonds shift for higher frequencies suggesting that  $SbPO_4$  is in a more distorted (more connected) arrangement. The same behavior occurs with respect to W-O<sub>t</sub> bonds. This fact is attributed to the substitution of trigonal  $SbO_3$  units (from  $Sb_2O_3$ ) for more voluminous octahedral  $WO_6$  units.

Raman results reinforce the structural model assumed for sbpw9 sample, as discussed above. The emerging band at 910  $cm^{-1}$  supports the existence of W-O<sub>t</sub> bonds coming from isolated  $WO_6$  units into the glass matrix. In fact, it means that there is almost no formation of  $WO_6$ - $WO_6$  units, what is evidenced by the low intensity of the W-O-W bond at 810  $cm^{-1}$ . In this sense, the increase of  $WO_3$  content leads to formation of such bonds and the relative intensity of the bond at 810  $cm^{-1}$  increases compared to that at 910  $cm^{-1}$ . Therefore, the formation of  $WO_6$ - $WO_6$  bonds does not rule out the possibility of formation of structures like those described for  $Na_2W_2O_7$ <sup>32</sup>.

In the Figure 4b and 4c is shown a tentative deconvolution of the spectra from samples sbpw9 (a) and sbpw5 (b) which correspond to the lower and upper concentration limits of  $WO_3$ , respectively. For sample sbpw9 it is not possible to observe the presence of the band around 720  $cm^{-1}$  (which corresponds to the symmetric stretching of W-O-W bonds) as observed in crystalline  $WO_3$ . On the other hand, in the upper concentration limit, the large band observed for sample sbpw5, could be deconvoluted in six bands. For sbpw5 it is observed the presence of the bond attributed to the bending mode of the  $PO_4$  group at 638  $cm^{-1}$ , as well as, the band centered at 725  $cm^{-1}$  which corresponds to the symmetric stretching of the W-O-W bond. The other four bands (816, 918, 970 and 1100  $cm^{-1}$ ) are

present in both samples. After the Raman study we can verify the intermediary character of  $\text{WO}_3$ . For lower contents it acts as a modifier and for higher contents (consequently, lower content of  $\text{Sb}_2\text{O}_3$ ) it has an important role as a glass former.

With respect to the chemical environment around antimony and phosphorous atoms, both  $^{31}\text{P}$  MAS NMR and XANES Sb-edges data show no substantial changes. NMR data show no anisotropy around the P atoms while just a small chemical shift was observed. XANES data from Sb- $L_1$  edge do not emphasize any significant change in the electronic density around the Sb atoms but rather shows the small increase of the intensity of the white line (insert of Figure 6). This effect is observed because antimony atoms in  $\text{SbPO}_4$  have four neighbors, while in  $\text{Sb}_2\text{O}_3$  they are surrounded by only three oxygen atoms. The picture obtained from XANES is the average of both  $\text{SbO}_3\text{E}^-$  and  $\text{SbO}_4\text{E}^-$  contributions<sup>29</sup>. Replacing  $\text{Sb}_2\text{O}_3$  by  $\text{WO}_3$ , the  $\text{SbO}_4\text{E}^-$  species plays a more important role in the intensity of the white line.

With respect to the tungsten environment, the scenario discussed above is also supported by XANES results at W- $L_1$  edge. The absence of the pre-peak 12108 eV in glasses confirms that tungsten atoms are present in the  $\text{WO}_6$  form. The sample sbpw9 presents a less pronounced shoulder at around 12111 eV according with the model proposed when  $\text{WO}_6$  units are dispersed in the glass matrix. In the same direction the sample sbpw14, present a more pronounced shoulder closest to that observed in  $\text{WO}_3$ .

## 5. Conclusions

Glasses have been prepared in a new ternary system  $\text{Sb}_2\text{O}_3\text{-SbPO}_4\text{-WO}_3$ . The incorporation of  $\text{WO}_3$  enhances the thermal stability of the glasses against devitrification when compared to the binary  $\text{Sb}_2\text{O}_3(0.6)\text{-SbPO}_4(0.4)$  composition. The connectivity of the network increases with  $\text{WO}_3$  content which is consistent with the high values of the glass transition temperature. Raman studies suggest that  $\text{WO}_3$  incorporation depolymerises the network constituted by antimony oxide while a second network containing  $\text{WO}_6$  octahedral units is build up. XANES in the W- $L_1$  edge for glasses confirms the presence of only octahedral units like those observed in crystalline  $\text{WO}_3$ . Such characteristics make these glasses suitable for studies for photo and electrochromic applications, as well as for solid state batteries. Both possibilities are currently under consideration.

## 6. Acknowledgments

The authors are grateful to grants #2013/07793-6, #2016/16343-2 and #2016/16900-9 São Paulo Research Foundation - FAPESP and CAPES for financial support.

## 7. References

- [1] M. Nalin, M. Poulain, Mi. Poulain, S. J. L. Ribeiro, Y. Messaddeq, *J. Non-Cryst. Sol.* 284 (2001) 110-116. [https://doi.org/10.1016/S0022-3093\(01\)00388-X](https://doi.org/10.1016/S0022-3093(01)00388-X).
- [2] G. Poirier, M. Poulain, Mi. Poulain, *J. Non-Cryst. Sol.* 284 (2001) 117-122. [https://doi.org/10.1016/S0022-3093\(01\)00389-1](https://doi.org/10.1016/S0022-3093(01)00389-1).
- [3] E. L. Falcão Filho, C. A. C. Bosco, G. S. Maciel, C. B. de Araujo, M. Nalin, Y. Messaddeq, *Appl. Phys. Lett.* 83 (2003) 1292-1294. <https://doi.org/10.1063/1.1601679>.
- [4] M. Nalin, Y. Messaddeq, S. J. L. Ribeiro, M. Poulain, V. Briois, G. Brunklaus, C. Rosenhahn, B. D. Mosel, H. Eckert, *J. Mater. Chem.* 14 (2004) 3398-3405. <https://doi.org/10.1039/B406075J>.
- [5] E. L. Falcão Filho, C. B. de Araujo, C. A. C. Bosco, G. S. Maciel, L. H. Acioli, M. Nalin, Y. Messaddeq, *J. Appl. Phys.* 97 (2005) 013505. <https://doi.org/10.1063/1.1828216>.
- [6] R. Makhoulfi, A. Boutarfaia, M. Poulain, *J. Alloy Comp.* 398 (2005) 249-252. <https://doi.org/10.1016/j.jallcom.2005.02.013>.
- [7] B. V. Raghavaiah, P. N. Rao, D. K. Rao, N. Veeraiah, *J. Phys. Chem. Sol.* 66 (2005) 954-962. <https://doi.org/10.1016/j.jpcs.2004.11.009>.
- [8] M. T. Soltani, T. Djouama, A. Boutarfaria, M. Poulain, *J. Optoelectron. Adv. M.* 1 (2009), 339-342. <https://s3.amazonaws.com/academia.edu.documents/41765931>.
- [9] C. Pereira, J. Barbosa, F. C. Cassanjes, R. R. Gonçalves, S. J. L. Ribeiro, G. Poirier, *Opt. Mater.* 62 (2016), 95-103. <https://doi.org/10.1016/j.optmat.2016.09.055>.



- [10] J. Li, Y. Zhang, S. Nian, Z. Wu, W. Cao, N. Zhou, D. Wang, *Appl. Phys.* 123 (2017), 00339-016. <https://doi.org/10.1007/s00339-016-0739-7>.
- [11] P. Petkova, K. Boubaker, P. Vasilev, M. Mustafa, A. Yumak, H. Touihri, M. Soltani, *AIP*, 1727 (2016) 020017. <https://doi.org/10.1063/1.4945972>.
- [12] D. Manzani, M. Montesso, C. F. Mathias, K. V. Krishanaiah, S. J. L. Ribeiro, M. Nalin, *Opt. Mater.* 57 (2016) 71-78. <https://doi.org/10.1016/j.optmat.2016.04.019>.
- [13] K. Ouannes, K. Lebbou, B. M. Walsh, M. Poulain, G. Alombert-Gotet, Y. Guyot, *Opt. Mater.* 65 (2017) 8-14. <https://doi.org/10.1016/j.optmat.2016.11.017>.
- [14] V. H. Rao, P. S. Prasad, P. V. Rao, L. F. Santos, N. Veeraiah, *J. Alloys Compd.* 687 (2016) 898-905. <https://doi.org/10.1016/j.jallcom.2016.06.256>.
- [15] Y. M. Sgibnev, N. V. Nikonorov, A. I. Ignatiev, *J. Lumin.* 188 (2017) 172-179. <https://doi.org/10.1016/j.jlumin.2017.04.028>.
- [16] D. Wang, J. Lu, Z. Zhang, Y. Hu, Z. Shen, *New J. Glass Cer.* 1 (2011) 34-38. <https://doi.org/10.4236/njgc.2011.12006>.
- [17] S. Y. Moustafa, M. R. Sahar, S. K. Ghoshal, *J. Alloys Compd.* 712 (2017) 781-794. <https://doi.org/10.1016/j.jallcom.2017.04.106>.
- [18] N. Shasmal, B. Karmakar, *J. Non-Cryst. Solids*, 463 (2017) 40-49. <https://doi.org/10.1016/j.jnoncrsol.2017.02.019>.
- [19] D. F. Franco, A. C. Sant'Ana, L. F. C. De Oliveira, M. A. P. Silva, *J. Mater. Chem. C* 3 (2015) 3803-3808. <https://doi.org/10.1039/C5TC00102A>.
- [20] T. Som, B. Karmakar, *Opt. Mater.* 31 (2009) 609-618. <https://doi.org/10.1016/j.optmat.2008.06.018>.
- [21] P. J. Miller, C. A. Cody, *Spectroch. Acta* 38A (1982) 555-559. [https://doi.org/10.1016/0584-8539\(82\)80146-3](https://doi.org/10.1016/0584-8539(82)80146-3).
- [22] M. Nalin, G. Poirier, Y. Messaddeq, S. J. L. Ribeiro, E. J. Carvalho, L. Cescato, *J. Non-Cryst. Sol.* 352 (2006) 3535-3539. <https://doi.org/10.1016/j.jnoncrsol.2006.03.087>.
- [23] G.I. Sincerbox, *Opt. Mat.* 4 (1995) 370-375. [https://doi.org/10.1016/0925-3467\(94\)00089-1](https://doi.org/10.1016/0925-3467(94)00089-1).
- [24] D. Strand, *J. Optoelec. Adv. Mat.* 7 (2005) 1679-1690. [https://joam.inoe.ro/arhiva/pdf7\\_4/Strand](https://joam.inoe.ro/arhiva/pdf7_4/Strand).
- [25] D. Psaltis, G. W. Burr, *Computer* 31 (1998) 52-60. <https://doi.org/10.1109/2.652917>.
- [26] P. Subbalakshmi, N. Veeraiah, *Phys. Chem. Glasses* 42 (2001) 307-314. <http://www.ingentaconnect.com/content/sgt/pcg/2001/0000042/F0020004/4204307>.
- [27] G. Poirier, M. Poulain, Y. Messaddeq, S. J. L. Ribeiro, *J. Non-Cryst. Sol.* 351 (2005) 293-298. <https://doi.org/10.1016/j.jnoncrsol.2004.11.017>.
- [28] G. Poirier, M. Nalin, Y. Messaddeq, S. J. L. Ribeiro, *Sol. State. Ionics*, 178 (2007) 871-875. <https://doi.org/10.1016/j.ssi.2007.01.012>.
- [29] M. Nalin, M. Poulain, Y. Messaddeq, S. J. L. Ribeiro, V. Briois, *J Optoelectr. Adv. Mat.* 3 (2001) 553-558. <http://hdl.handle/11449/32534>.
- [30] A. Dietzel, *Glasstech. Ber.* 22 (1968) 41-50. <https://pure.tue.nl/ws/files/1766128/23899>.
- [31] M. Nalin, G. Poirier, S.J.L. Ribeiro, Y. Messaddeq, L. Cescato, *J. Non-Cryst. Sol.*, 353 (2007) 1592-1597. <https://doi.org/10.1016/j.jnoncrsol.2007.01.031>.
- [32] P. Charton, PhD thesis, Université de Montpellier 2, France (2002).
- [33] C. Guéry, C. Choquet, F. Dujeancourt, J. M. Tarascon, J.C. Lassègues, *J. Sol. State Electrochem.* 1 (1997) 199-204. <https://doi.org/10.1007/s100080050049>.
- [34] J. M. Durand, P. E. Lippens, F. J. Olivier, J. C. Jumas, M. Womes, *J. Non-Cryst. Sol.*, 194 (1996) 109-121. [https://doi.org/10.1016/0022-3093\(95\)00507-2](https://doi.org/10.1016/0022-3093(95)00507-2).
- [35] M. Maczka, L. Kempinski, J. Hanusa, S. Kojima, *J. Non-Cryst. Sol.*, 353 (2007) 4681-4690. <https://doi.org/10.1016/j.jnoncrsol.2007.06.064>.
- [36] A. L. Greer, *Nature*, 366 (1993) 303-304. <https://doi.org/10.1038/366303a0>.